ISSN: 2633-4828 Vol. 5, No. 3, September 2023

International Journal of Applied Engineering and Technology

A Silicon-on-Insulator 4x4 Multimode Interference (MMI) Based Microring Structure for Highly Sensitive Hydrogen Detection

Trung Thanh Le[1], Duy Tien Le[2], Anh Tuan Nguyen[3]

[1,2,3]*International School (VNU-IS), Vietnam National University (VNU), Hanoi, Vietnam*

Email: thanh.le@vnu.edu.vn

Thi Hong Loan Nguyen[4]

[4]*University of Natural Resources and Environment, Hanoi, Vietnam*

Duong The Do[5]

[5]*Academy of Policy and Development, Hanoi, Vietnam*

Date of Submission: 13th August 2023 Revised: 29th September 2023 Accepted: 9th Oct 2023

How to Cite: **Trung Thanh Le, Duy Tien Le, Anh Tuan Nguyen, Thi Hong Loan Nguyen and Duong The Do (2023). A Silicon-on-Insulator 4x4 Multimode Interference (MMI) Based Microring Structure for Highly Sensitive Hydrogen Detection. International Journal of Applied Engineering and Technology 5(3), pp.106-113.**

Abstract **- We propose a highly sensitive hydrogen sensor structure using silicon waveguide. Based on the Fano like effect generated from the 4x4 MMI resonator structure integrated with one microring resonator, the shift of resonance wavelength with the presence of the hydrogen is achieved with 40 orders higher than the typical sensor based on single microring resonator and Mach Zehnder Interferometer (MZI). The device is highly sensitive to low hydrogen concentration variations of from 0-4% in the range of hydrogen's lower flammability limit (EFL). We also optimally design the gap and width of the palladium (Pd) covered in the sensing area for low loss, but still achieve the low detection limit and high sensitivity. This optical hydrogen sensor can provide capabilities for ease of fabrication, ease of fabrication, low fabrication tolerance compared with optical sensors based on only directional couplers.**

Index Terms **- Optical sensor, multimode interference, microring resonator, integrated optics, hydrogen detection.**

INTRODUCTION

Hydrogen has found widespread use as a fuel source across various industries, including chemical production, oil refineries, gas refineries, aerospace, and the automotive sector [1]. When hydrogen boasts a sufficiently high calorific value, it can emerge as a competitive means of energy transport. However, it's important to acknowledge that public utilization and storage of hydrogen come with inherent risks. An elevated concentration of hydrogen exceeding the lower flammability limit (4%) can lead to a severe explosion [2]. Therefore, the development of a fast and dependable gas sensor for hydrogen detection is crucial to ensure its safe storage, handling, and utilization.

Some methods of hydrogen sensors has been proposed in the literature such as encompassing catalytic, electrochemical, metal-oxide semiconductor, and optical hydrogen sensors [3]. Among these, optical sensors provide several advantages because of compact size, safety features, and immunity to electromagnetic interference. In recent years, optical fiber-based hydrogen sensors represent emerging technologies with notable sensitivity and multiplexing capabilities. However, their bulkiness limits their suitability for seamless integration [4]. The ability to integrate these sensors offers numerous benefits, including enhanced compactness and cost-effective large-scale integration packaging.

The Silicon-on-Insulator (SOI) platform stands out as an exceptional choice for integrating optical sensors due to its remarkable compactness and compatibility with complementary metal-oxide-semiconductor (CMOS) fabrication technologies [5]. This compatibility holds promise for the seamless integration of electronic and photonic devices on a single platform. Furthermore, SOI offers an excellent foundation for consolidating numerous sensing elements onto a single microchip.

Numerous optical hydrogen sensors based on Silicon-on-Insulator (SOI) technology have been created, incorporating key sensing components such as microring resonators, Mach Zehnder Interferometer [2, 6, 7]. One noteworthy example is a Pd-based ridge-waveguide optical hydrogen sensor that has been extensively documented in scientific literature [8]. This sensor functions by detecting the presence of hydrogen and quantifying its concentration by tracking alterations in light intensity at a specific wavelength.

Its straightforward and dependable operation is attributed to the direct measurement of intensity, negating the necessity for an extra spectrum analyzer.

It's worth highlighting that in prior research endeavors, exclusively transverse electric (TE) mode-polarized light from a tunable laser was employed, and the underlying principles governing this TE mode-based sensing approach were not exhaustively investigated. In our current study, our objective is to enhance the sensor's performance such as high sensitivity. To accomplish this, we have introduced an innovative sensor configuration while presenting an in-depth exploration of the core sensing principles involved.

In our current design, the fundamental sensor element utilized is a Surface Plasmon Interferometer (SPI), which incorporates a thin Pd layer embedded within the Silicon-on-Insulator (SOI) microring resonator's waveguide. Owing to its exceptional integration and compactness, the SPI hydrogen sensor possesses a competitive edge when compared to other hydrogen sensors that rely on SOI technology. We foresee that this pioneering approach will pave the way for novel possibilities and significantly enhance the adaptability of hydrogen sensing based on SOI technology.

Except for fiber optic sensors, many of the hydrogen sensors discussed earlier face constraints on their operational lifespan due to issues related to electrical corrosion. Furthermore, certain sensors among these can present risks in potentially explosive environments due to the potential for spark generation. While fiber optic sensors effectively mitigate most of these shortcomings, they are hindered by limitations in terms of integration, primarily stemming from their relatively large physical dimensions.

Furthermore, hydrogen-sensitive materials such as palladium (Pd) and platinum (Pt) demonstrate exceptional adhesion properties when integrated with silicon ring resonators. These ultra-compact optical sensors not only exhibit environmental compatibility but also excel in challenging and combustible environments. In the realm of hydrogen sensors, the selected materials must satisfy three fundamental criteria: sensitivity, selectivity, and specificity, all of which are met by palladium (Pd) and platinum (Pt). Both Pd and Pt are ideal choices for hydrogen sensing due to their propensity to engage in reactions with hydrogen, resulting in Pd hydride-based hydrogen sensors integrated with micro ring resonators. These sensors possess the remarkable capability to detect low hydrogen concentrations ranging from 0% to 4%.

Moreover, our sensor structure is based on multimode interference (MMI) theory and is seamlessly integrated with microring resonators. Consequently, this design achieves a compact form factor, excellent fabrication tolerance, a high free spectral range (FSR), and minimal optical loss. The core of this design features a hydrogen-sensitive Pd layer positioned within the inner layer of the micro ring resonator, ensuring precise and efficient hydrogen detection.

We present a new optical sensor structure for hydrogen detection in this research. The new structure is based on MMI coupler integrated with one microring resonator covered with Pd material. Our structure can generate the Fano line shape for sensing principles [9]. Therefore, it can provide a ultra-high sensitivity compared with the sensing structures based on microring resonator and MZI in the literature. In our current research, we are introducing an innovative solution—a silicon-based on-chip optical micro ring resonator based on 4x4 MMI hydrogen sensor. This sensor has the potential to address numerous limitations associated with existing sensors. Notably, it boasts an ultra-compact size, enabling effortless integration, and offers high sensitivity. This advancement holds the promise of revolutionizing hydrogen sensing technology, enhancing both safety and performance in various applications.

DEVICE STRUCTURE AND SENSING PRINCIPLE

The new sensor structure is shown in Fig. 1(a). It consist of a 4x4 MMI coupler. Here, a_i, b_i (i=1,...,4) are complex amplitudes. A microring resonator covered with Pd material for H2 sensing is used. For single mode operation, the silicon waveguide has a height of 220nm, width of 500nm. The wavelength is at 1550nm. The silica is used for cladding cover at the reference resonator. The analyte is used as cladding at the sensing region. The core structure consists of a silicon-based micro-ring resonator featuring a thin layer of hydrogen-sensitive material (palladium in this design), applied to its inner surface. A microring resonator covered with the Pd material is located at the arm of the MMI coupler as shown in Fig.1(b).

The layer hydrogen sensitive material Pd of width 400nm is deposited on the inner surface of the ring resonator. For MMI design, the locations of input and output waveguides are located at special locations as follows [10]:

$$x_i = (i+\frac{1}{2})\frac{W_{MMI}}{N}, (i=0,1,\ldots,N-1) \qquad (1)$$

For mode propagation method, the length of 4x4 MMI coupler is of $L_{MMI} = \frac{3L_\pi}{2}$ [11-14]. In our design, the width of the MMI is W_{MMI} =6μm for compactness. By using the BPM (Beam propagation method), the optimal length of the 4x4 MMI coupler is $L_{MMI} = 138.9\ \mu m$.

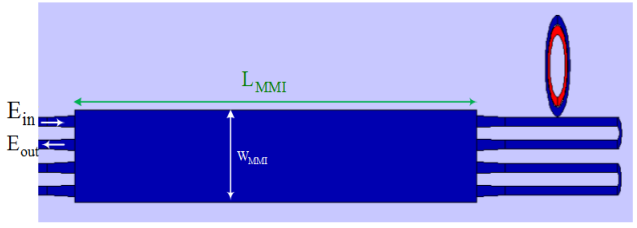

(a)

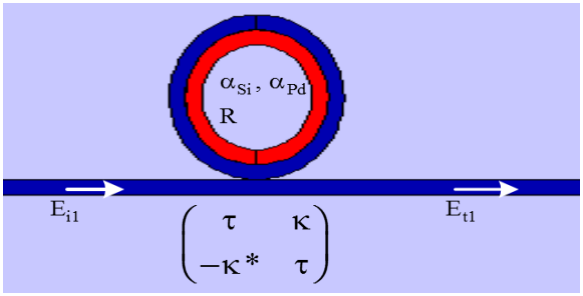

(b)

Fig. 1 (a) Hydrogen sensor based on 4x4 MMI coupler with microring resonator covered with Pd material, (b) microring resonator covered with Pd material

MMI coupler can characterized by a matrix [15]. The phase ϕ_{ij} associated with imaging an input i to an output j in an MMI coupler. These phases ϕ_{ij} form a matrix S_{4x4}, with i representing the row number, and j representing the column number [10]. The proposed MMI coupler in this research has the following transfer matrix [14]

$$S_{4x4MMI} = \frac{1}{2}\begin{bmatrix} 1-j & 0 & 0 & 1+j \\ 0 & 1-j & 1+j & 0 \\ 0 & 1+j & 1-j & 0 \\ 1+j & 0 & 0 & 1-j \end{bmatrix} \quad (2)$$

When the concentration of hydrogen in the surrounding environment rises, palladium undergoes a chemical change that leads to the creation of palladium hydride. This transformation induces alterations in the effective refractive index of the palladium layer. Notably, both the real and imaginary components of the refractive index experience variations in response to fluctuations in hydrogen concentration within the surrounding environment. When measuring the refractive index of palladium hydride, it becomes evident that both the real and imaginary components of this index undergo changes when the concentration of hydrogen gas ranges from 0% to 4%. It is worth highlighting that for every 1% modification in hydrogen concentration, the corresponding adjustment in the refractive index of palladium hydride follows a nearly linear pattern.

In this design, we use the Pd film thickness of 60. The field profile of the waveguide is shown in Fig. 2(a) calculated by finite difference method (FDM)[16]. Fig. 2(b) shows signal propagation via the microring resonator covered with the Pd material.

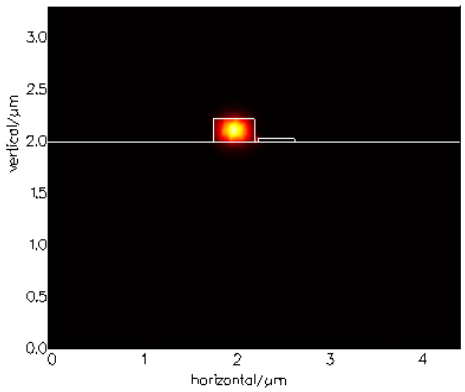

(a)

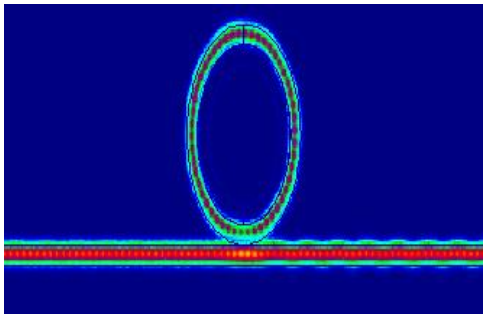

(b)

Fig. 2 Mode profile of the waveguide covered with Pd material and propagation via a microring resonator

At the specified palladium (Pd) thickness, the complex refractive index (RI) for the Pd layer at a wavelength of 1550 nm is determined to be 3.605 + j8.498. Fig. 3 illustrates the variations of both the real and imaginary parts of the Pd refractive index with respect to wavelength. It's important to note that the real and imaginary components of the Pd refractive index exhibit significant fluctuations with changes in film thickness. This phenomenon is particularly pronounced for film thicknesses where the film becomes partially transparent. In such cases, the imaginary part of the refractive index tends towards 'zero,' signifying reduced light absorption, while the real part tends towards '1,' indicating a trend towards transparency, as the film thickness approaches very small values. This behaviour reflects the complex optical properties of the Pd layer, especially in the context of its interaction with light at a specific wavelength of 1550 nm.

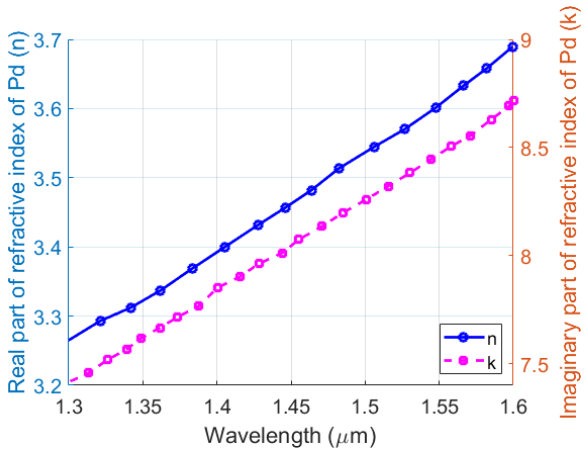

Fig. 3 Refractive index of Pd material at different wavelengths

Fig. 4 shows a plot of real and imaginary parts (n, k) of Pd refractive index versus thickness for a wavelength of 1550 nm.

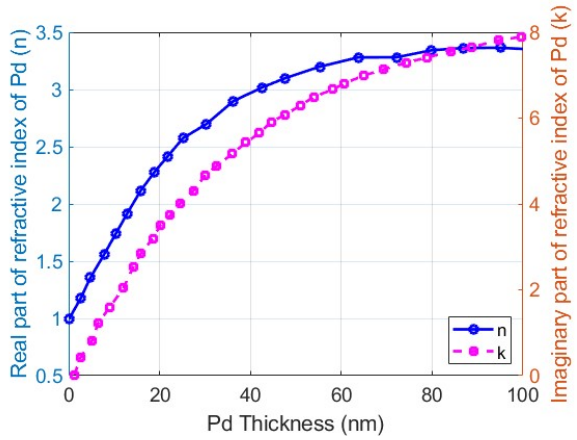

Fig. 4 Refractive index of Pd material at different wavelengths

The adsorption of hydrogen onto the palladium (Pd) layer results in changes to its refractive index (RI), which, in turn, causes shifts in the resonance wavelength. However, there exist varying reports regarding the percentage change in the refractive index of the Pd layer in response to hydrogen adsorption.

It is established that as hydrogen is adsorbed, both the real (ε1) and imaginary (ε2) parts of the permittivity of the Pd films decrease. These changes in permittivity are directly associated with the alterations in the real (n) and imaginary (k) parts of the refractive index:

$$n = \sqrt{\frac{\sqrt{\varepsilon_1^2 + \varepsilon_2^2} + \varepsilon_1}{2}} \text{ and } k = \sqrt{\frac{\sqrt{\varepsilon_1^2 + \varepsilon_2^2} - \varepsilon_1}{2}} \quad (3)$$

Thus if ε1 and ε2 decrease, n will also decrease and k may increase or decrease depending on the value of the permittivity. The real part of the Pd refractive index will decrease on hydrogen adsorption. The complex permittivity of the Pd after hydrogen exposure can be modelled as the following simple equation

$$\varepsilon(Pd, \%H_2) = h(\%H_2) x \varepsilon(Pd, 0\%H_2) \quad (4)$$

Where $\varepsilon(Pd, 0\%H_2)$ is the complex permittivity of the pure Pd layer and $h(\%H_2)$ is the function depending on hydrogen concentration, temperature and humidity. The real and imaginary parts of Pd refractive index hydrogen from 0-4% are simulated in Fig. 5(a). Fig. 5(b) shows the loss factor, respectively.

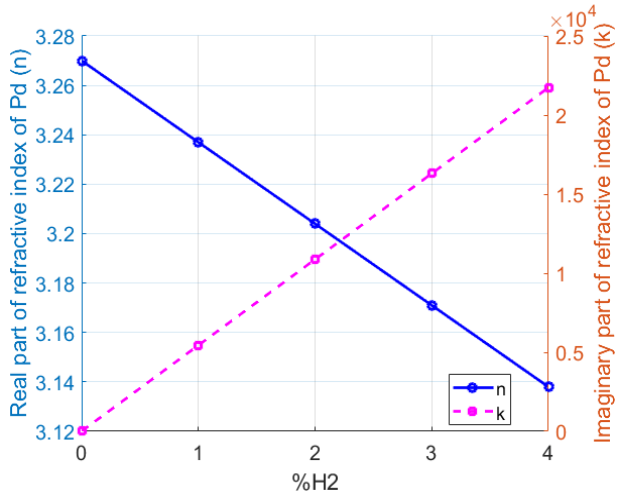

(a)

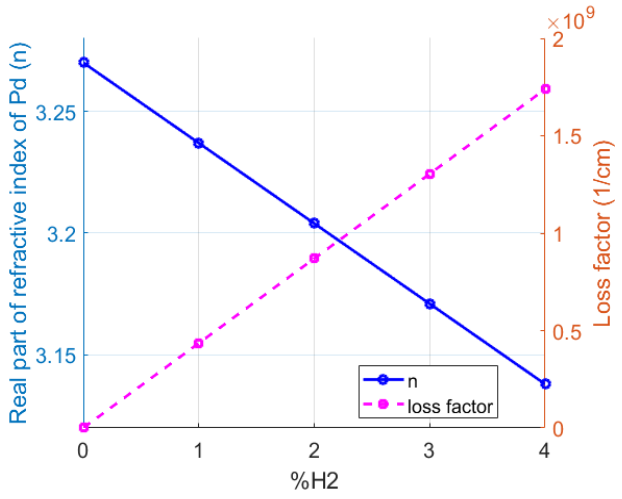

(b)

Fig. 5 (a) Refractive index of Pd with different concentration of H2, (b) Loss factor

The gap between the silicon waveguide and the Pd layer is strongly effects on the performance of the sensor. If the gap is too small, the loss shall increase but the sensitivity is reduced. As a result, we need to optimize the gap. The effective index calculated by the EME method at different gap is shown in Fig. 6(a). The loss factor at different gaps is simulated in Fig.6(b). The simulation results show that the optimal gap is should be at around 10nm.

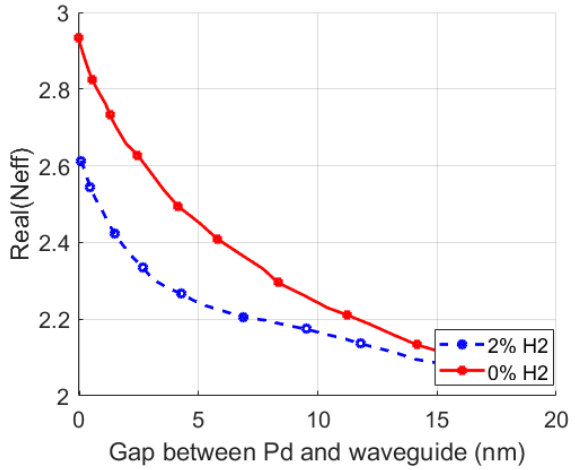

(a)

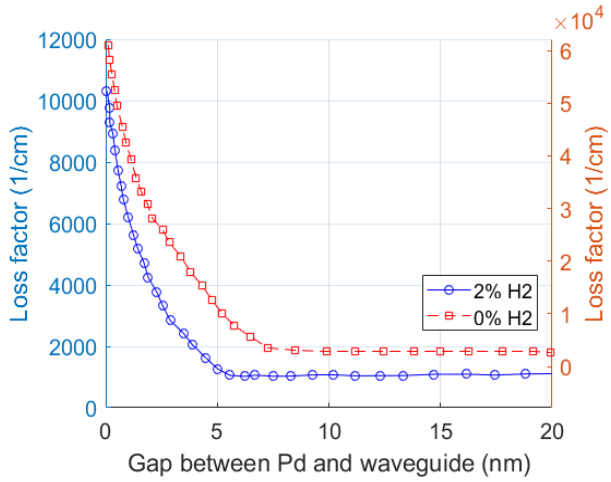

(b)

Fig. 6 Effective refractive index of Pd sensing with hydrogen and loss factor at different gap distance between the silicon waveguide and Pd layer

For a microring resonator, the fields at output of the microring resonator in the sensing area of Fig.1(b) is expressed by using the Yariv's model [17]:

$$\begin{pmatrix} E_{t1} \\ E_{t2} \end{pmatrix} = \begin{pmatrix} \tau & \kappa \\ -\kappa^* & \tau \end{pmatrix} \begin{pmatrix} E_{i1} \\ E_{i2} \end{pmatrix} \quad (5)$$

where κ and τ coefficients of the directional coupler; $E_{i2} = \alpha \exp(j\phi) E_{t2}$, α is the loss factor of the field after one round trip through the microring resonator; n_{eff} and L_R is effective refractive index and length of the resonator.

The loss factor of the Pd covered microring resonator can be expressed by:

$$\alpha = \exp(-0.5\alpha_{Pd} L_{Pd}) \exp[-0.5\alpha_{Si}(2\pi R - L_{Pd})] \quad (6)$$

where R is the radius of the microring and α_{Si} (dB / cm) is the loss coefficient of the Si waveguide.

The output field and input field of a single microring resonator is:

$$E_{t1} = E_{i1} \frac{-\alpha + \tau e^{-j\phi}}{-\alpha\tau^* + e^{-j\phi}} \quad (7)$$

Where

$E_{i2} = \alpha \exp(j\varphi) E_{t2}$,

$\varphi = \frac{2\pi}{\lambda}[n_{eff}^{Pd} L_{Pd} + n_{eff}^{Si}(2\pi R - L_{Pd})]$ is the round trip phase.

As a result, the output power is [17]:

$$T = \left|\frac{E_{t1}}{E_{i1}}\right|^2 = \frac{\alpha^2 - 2\alpha\tau\cos(\varphi) + \tau^2}{1 - 2\alpha\tau\cos(\varphi) + \alpha^2\tau^2} \quad (8)$$

The phase of the resonator is [18]

$$\phi_{single} = artan\left\{\frac{\alpha\kappa^2 \sin(\omega)}{\left(1+\alpha^2\right)\tau - \left(1+\tau^2\right)\alpha\cos(\omega)}\right\} \quad (9)$$

where $\omega = \frac{c}{\lambda}$ is the angular frequency. For the ring resonator, resonance conditions meet the following requirement:

$$m\lambda_r = n_{eff} L_R = n_{eff}(\pi R) \quad (10)$$

where λ_r is the resonance wavelength and m is an integer representing the order of the resonance.

The operation of the sensor using the proposed MMI resonator is based on the shift of resonance wavelength. The evanescence field, which represents the portion of light that is penetrating inside the surrounding material in the sensing area, can interact with the analytes. A small change in the effective refractive index n_{eff} will result in a shift in the resonance.

The alteration in the effective index occurs as a consequence of fluctuations in the ambient refractive index (n_a) brought about by the presence of analytes within the microring. The sensitivity of the sensor, based on the shift in resonance wavelength, can be expressed as follows [19, 20]

$$S = \frac{\partial\lambda_r}{\partial n_a} = \frac{\partial\lambda_r}{\partial n_{eff}} \frac{\partial n_{eff}}{\partial n_a} = \frac{\partial\lambda_r}{\partial n_{eff}} S_W \text{ (nm/ RIU)} \quad (11)$$

where $S_W = \frac{\P n_{eff}}{\P n_a}$ is the sensitivity of the waveguide and RIU is refractive index unit.

We find out the transmittance of the structure in Fig.1(a) as follows:

$$T = \left| \cos\left(\frac{1}{2}\arctan\left\{\frac{\alpha\kappa^2\sin(\omega)}{\left(1+\alpha^2\right)\tau-\left(1+\tau^2\right)\alpha\cos(\omega)}\right\}\right)\right|^2 \qquad (12)$$

Using equation (8), the spectral transmission of the sensor is shifted when the analytes are presented. By measuring the shift of the resonance wavelength, the concentration of the analyte solutions can be detected.

SIMULATION RESULTS AND DISCUSSIONS

The transmission characteristics of the sensor configuration in Fig.1(a) are presented in Fig.7 for different coupling coefficients of the microring resonator and Fig.8 for different ring waveguide radii respectively. For a larger coupling coefficient, the steeper Fano shape can be achieved. However, the fabrication is much more difficult for the ring resonator due to the requirement of smaller gap of the directional coupler. Therefore, the 3dB coupler can be used for practical applications.

The FDTD simulations of field propagation through the device at the peak and dip wavelengths of the Fano resonance are shown in Figure 5(b) and (c), where the Fano resonance shape can be expressed by the universal formula for a scattering cross section [21]:

$$F(\varepsilon) = \frac{(\varepsilon+q)^2}{\varepsilon^2+q} \qquad (13)$$

Where q is the shape parameter, ε is the reduced energy. The proposed structure can produce the Fano profile (transmission input port 1, output port 1) compared with the Fano resonance profile for q=±1. Now, we consider the ring resonator. The transmittance of the resonator is obtained by

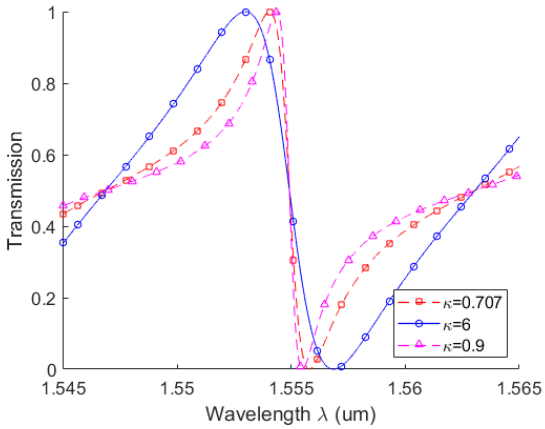

Fig. 7. The Fano shape of the sensor configuration achieved at different coupling coefficients of the directional coupler at the microring resonator

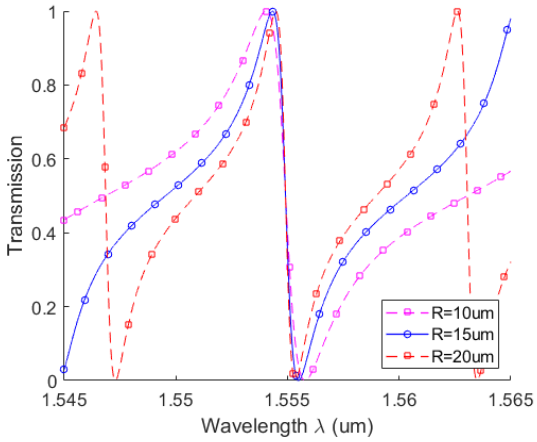

Fig. 8. The Fano shape of the sensor configuration achieved at different radii of the ring waveguide of the microring resonator

The simulations presented in Fig. 8 reveal that as the radius of the ring structure increases, the Fano resonance shape becomes steeper. Furthermore, larger ring radii result in reduced optical losses within the ring, making fabrication of the device more feasible. However, there is a trade-off to consider. While larger ring radii create steeper Fano resonances and offer advantages in terms of fabrication and reduced optical losses, they also lead to a limitation in the detection range. This limitation arises from the reduced free spectral range (FSR) of the device when used for sensor applications. The FSR essentially represents the range of wavelengths over which the device can operate effectively without overlapping resonances. To strike a balance between these factors, a suitable radius (likely neither too small nor too large) is chosen for the ring structure. This choice aims to optimize the device's performance, taking into account factors such as sensitivity, fabrication feasibility, and the desired detection range for specific sensor applications.

In Fig.9, the transmission characteristics of the device are simulated. This simulation provides valuable information regarding the relationship between the concentration of hydrogen gas (H2) and the shift in resonance wavelength. By carefully analyzing the data from this simulation, it is possible to establish a direct relationship between the concentration of H2 gas in the environment and the corresponding shift in the resonance wavelength of the device. This shift in resonance wavelength is influenced by the interaction between the H2 gas and the device, causing changes in its optical properties.

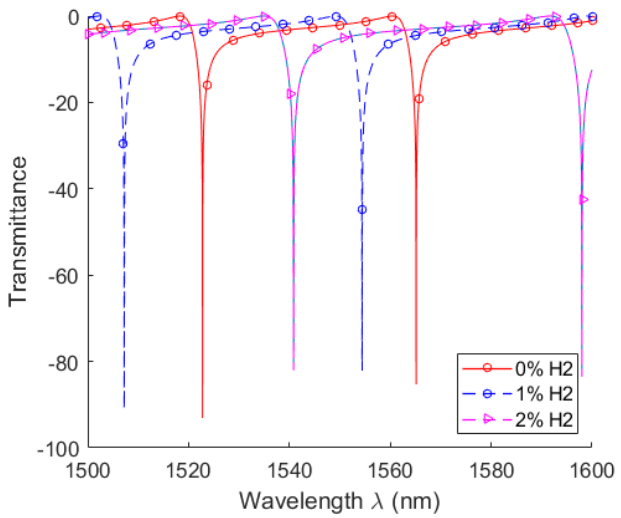

Fig 9. Transmission of the H2 sensor

Finally, we compared our design with the conventional design based on MZI structure in Fig.10. The sensitivity of the sensor based on the conventional microring resonator is also presented in Fig.10. We can see that the sensitivity of the proposed configuration is much higher than the conventional one (about 10 times). The sensitivity is about 4nm per 1% hydrogen compared with 0.35nm per 1% hydrogen in the literature.

In this study, we use the resonance wavelength shift based mechanism for sensor, the sensitivity of the sensor can be calculated by

$$S = \frac{\Delta\lambda}{\Delta n} = 285(\text{nm/ RIU}) \qquad (14)$$

The new sensor can provide higher sensitivity compared with the published sensor with sensitivity of 170nm/RIU [22]. If we use the optical refractometer with a resolution of 20pm, the detection limit of our sensor is about $2.1\text{x}10^{-5}$, compared with a detection limit of $1.78\text{x}10^{-5}$ of single microring resonator sensor.

To evaluate the performance of the proposed sensing configuration, the figure of merit is presented. The FOM of the sensor is

$$\text{FOM} = \frac{S}{\text{FWHM}} \qquad (15)$$

Where S the sensitivity of the sensor and FWHM is the fullwidth at half maximum. Therefore, we can calculate the FoM=52.This FOM is greater than that of the previous reports [23].

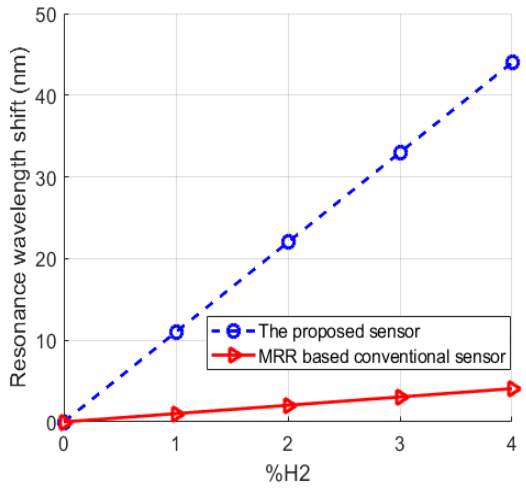

Fig. 10. Resonance wavelength shift at different H2 concentration

The overal simulations of the sensing structure are shown in Fig. 8 at different wavelengths.

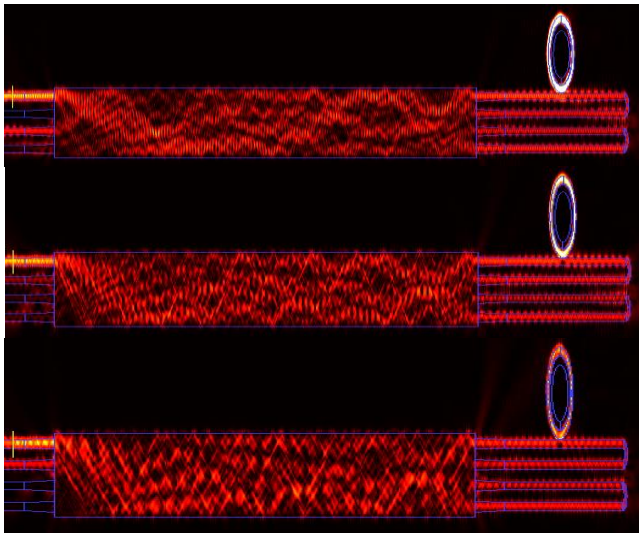

Fig 11. Transmission of the H2 sensor

CONCLUSION

This study has presented a new structure for hydrogen sensor based on only one 4x4 MMI coupler integrated with a microring resonator covered with the Pd material. The high sensitivity of 285 nm/RIU and low detection limit of $2.1\text{x}10^{-5}$ can be achieved. The sensor was designed using silicon waveguide that is cheap and compatible with the current existing CMOS technology.

ACKNOWLEDGEMENTS

This research is funded by Vietnam National University, Hanoi (VNU) under project number QG.19.58.

REFERENCES

[1] A. K. Pathak, S. Verma, N. Sakda, C. Viphavakit, R. Chitaree, and B. M. A. Rahman, "Recent Advances in Optical Hydrogen Sensor including Use of Metal and Metal Alloys: A Review," Photonics, vol. 10, no. 2, doi: 10.3390/photonics10020122.

[2] S. Matsuura, N. Yamasaku, Y. Nishijima, S. Okazaki, and T. Arakawa, "Characteristics of Highly Sensitive Hydrogen Sensor Based on Pt-WO3/Si Microring Resonator," Sensors, vol. 20, no. 1, 2020, doi: 10.3390/s20010096.

[3] S. Garg, V. Mishra, L. F. Vega, R. S. Sharma, and L. F. Dumée, "Hydrogen Biosensing: Prospects, Parallels, and Challenges," Industrial & Engineering Chemistry Research, vol. 62, no. 11, pp. 4676-4693, 2023/03/22 2023, doi: 10.1021/acs.iecr.2c03965.

[4] N. A. Yebo, Taillaert, D. Roels, and D. Lahem, "Silicon-on-Insulator (SOI) Ring Resonator-Based Integrated Optical Hydrogen Sensor," IEEE Photonics Technology Letters, vol. 21, no. 14, pp. 960 - 962, 2009.

[5] M. Shahbaz, M. A. Butt, and R. Piramidowicz, "Breakthrough in Silicon Photonics Technology in Telecommunications, Biosensing, and Gas Sensing," Micromachines, vol. 14, no. 8, doi: 10.3390/mi14081637.

[6] N. Bavili et al., "Highly sensitive optical sensor for hydrogen gas based on a polymer microcylinder ring resonator," Sensors and Actuators B: Chemical, vol. 310, p. 127806, 2020/05/01/ 2020, doi: https://doi.org/10.1016/j.snb.2020.127806.

[7] Y.-n. Zhang, H. Peng, X. Qian, Y. Zhang, G. An, and Y. Zhao, "Recent advancements in optical fiber hydrogen sensors," Sensors and Actuators B: Chemical, vol. 244, pp. 393-416, 2017/06/01/ 2017, doi: https://doi.org/10.1016/j.snb.2017.01.004.

[8] Y. S. Yi, D. C. Wu, P. Birar, and Z. Yang, "Ring Resonator-Based Optical Hydrogen Sensor," IEEE Sensors Journal, vol. 17, no. 7, pp. 2042-2047, 2017, doi: 10.1109/JSEN.2017.2669521.

[9] T.-T. Bui and T.-T. Le, "Glucose sensor based on 4x4 multimode interference coupler with microring resonators," in 2017 International Conference on Information and Communications (ICIC), Hanoi, Vietnam, 26-28 June 2017 2017: IEEE, pp. 224-228, doi: 10.1109/INFOC.2017.8001679.

[10] T.-T. Le and L. Cahill, "Generation of two Fano resonances using 4x4 multimode interference structures on silicon waveguides," Optics Communications, vol. 301-302, pp. 100-105, 2013.

[11] D.-T. Le and T.-T. Le, "Fano Resonance and EIT-like effect based on 4x4 Multimode Interference Structures," International Journal of Applied Engineering Research, vol. (accepted for publication), 2017.

[12] D.-T. Le, T.-D. Do, V.-K. Nguyen, A.-T. Nguyen, and T.-T. Le, "Sharp Asymmetric Resonance Based on 4x4 Multimode Interference Coupler," International Journal of Applied Engineering Research, vol. (accepted for publication in 2017), 2017.

[13] T.-T. Le, "Two-channel highly sensitive sensors based on 4 × 4 multimode interference couplers," Photonic Sensors, pp. 1-8, DOI: 10.1007/s13320-017-0441-1, 2017. [Online]. Available: https://doi.org/10.1007/s13320-017-0441-1.

[14] T.-T. Le and L. Cahill, "The Design of 4×4 Multimode Interference Coupler Based Microring Resonators on an SOI Platform," Journal of Telecommunications and Information Technology, Poland, pp. 98-102, 2009.

[15] T.-T. Le, Multimode Interference Structures for Photonic Signal Processing. LAP Lambert Academic Publishing, 2010.

[16] Y.-C. Chiang, Y.-P. Chiou, and H.-C. Chang, "Improved Full-Vectorial Finite-Difference Mode Solver for Optical Waveguides With Step-Index Profiles," Journal of Lightwave Technology, vol. 20, no. 8, p. 1609, 2002/08/01 2002. [Online]. Available: http://jlt.osa.org/abstract.cfm?URI=jlt-20-8-1609.

[17] A. Yariv, "Universal relations for coupling of optical power between microresonators and dielectric waveguides," Electronics Letters, vol. 36, pp. 321–322, 2000.

[18] D.-T. Le, M.-C. Nguyen, and T.-T. Le, "Fast and slow light enhancement using cascaded microring resonators with the Sagnac reflector," Optik - International Journal for Light and Electron Optics, vol. 131, pp. 292–301, Feb. 2017.

[19] C.-Y. Chao and L. J. Guo, "Design and Optimization of Microring Resonators in Biochemical Sensing Applications," IEEE Journal of Lightwave Technology, vol. 24, no. 3, pp. 1395-1402, 2006.

[20] T.-T. Le, "Realization of a Multichannel Chemical and Biological Sensor Using 6x6 Multimode Interference Structures," International Journal of Information and Electronics Engineering, Singapore, vol. 2, pp. 240-244, 2011.

[21] A. E. Miroshnichenko, S. Flach, and Y. S. Kivshar, "Fano resonances in nanoscale structures," Review Modern Physics, vol. 82, pp. 2257-, Aug. 2010.

[22] O. A. Marsh, Y. Xiong, and W. N. Ye, "Slot Waveguide Ring-Assisted Mach–Zehnder Interferometer for Sensing Applications," IEEE Journal of Selected Topics in Quantum Electronics, vol. 23, no. 2, pp. 440-443, 2017, doi: 10.1109/jstqe.2016.2617084.

[23] Z. Chen, L. Yu, L. Wang, G. Duan, Y. Zhao, and J. Xiao, "A Refractive Index Nanosensor Based on Fano Resonance in the Plasmonic Waveguide System," IEEE Photonics Technology Letters, vol. 27, no. 16, pp. 1695-1698, 2015, doi: 10.1109/lpt.2015.2437850.

AUTHOR'S INFORMATION

Trung Thanh Le, Associate Professor, PhD in electronic and telecommunicaton engineering at Vietnam National University (VNU), Hanoi, Vietnam. Email: thanh.le@vnu.edu.vn, Phone: +84 9851425788

Duy Tien Le received MSc degrees of Information Systems in 2014 from Hanoi VNU University of Engineering and Technology. He is a currently PhD student of Computer Engineering, Posts and Telecommunications Institute of Technology (PTIT), Hanoi, Vietnam. His research interests include DSPs and Photonic Integrated Circuits.

Anh Tuan Nguyen is a currently PhD student Vietnam Academy of Science and Technology, Hanoi, Vietnam. His research interests include optical sensor and GIS integration with optical sensors.

Thi Hong Loan Nguyen is a lecturer at Hanoi University of Natural Resources and Environment, Hanoi, Vietnam. She is pursuiting the PhD in computer engineering at Vietnam National University, Hanoi, Vietnam.

Duong The Do is a lecturer at Academy of Policy and Development, Hanoi, Vietnam.